catalysts

MDPI

Article

Role of N-Terminal Extensional Long α-Helix in the Arylesterase from *Lacticaseibacillus rhamnosus* GG on Catalysis and Stability

Bin-Chun Li *, Tongtong Guo, Xue Li, Xueting Hou and Guo-Bin Ding

Institute of Biotechnology, Key Laboratory of Chemical Biology and Molecular Engineering of Ministry of Education, Shanxi University, Taiyuan 030006, China
* Correspondence: libinchun@sxu.edu.cn; Tel.: +86-351-7011499

Abstract: In the α/β hydrolases superfamily, the extra module modulated enzymatic activity, substrate specificity, and stability. The functional role of N-terminal extensional long α-helix (Ala2-Glu29, designated as NEL-helix) acting as the extra module in the arylesterase LggEst from *Lacticaseibacillus rhamnosus* GG had been systemically investigated by deletion mutagenesis, biochemical characterization, and biophysical methods. The deletion of the NEL-helix did not change the overall structure of this arylesterase. The deletion of the NEL-helix led to the shifting of optimal pH into the acidity and the loss of thermophilic activity. The deletion of the NEL-helix produced a 10.6-fold drop in catalytic activity towards the best substrate *p*NPC10. NEL-Helix was crucial for the thermostability, chemical resistance, and organic solvents tolerance. The deletion of the NEL-helix did not change the overall rigidity of enzyme structure and only reduced the local rigidity of the active site. Sodium deoxycholate might partially replenish the loss of activity caused by the deletion of the NEL-helix. Our research further enriched the functional role of the extra module on catalysis and stability in the α/β hydrolase fold superfamily.

Keywords: α/β hydrolase; long α-helix; arylesterase; catalysis; stability

Citation: Li, B.-C.; Guo, T.; Li, X.; Hou, X.; Ding, G.-B. Role of N-Terminal Extensional Long α-Helix in the Arylesterase from *Lacticaseibacillus rhamnosus* GG on Catalysis and Stability. *Catalysts* **2023**, *13*, 441. https://doi.org/10.3390/catal13020441

Academic Editors: Ruizhi Han and Gopal Patel

Received: 3 February 2023
Revised: 15 February 2023
Accepted: 16 February 2023
Published: 18 February 2023

1. Introduction

As a rapidly growing enzyme family, the α/β hydrolase fold superfamily is highly diverse in sequence, but shares a common fold and a similar active center [1,2]. Most α/β hydrolases contain two domains, the conserved catalytically active core domain and an extra domain which is a cap, a lid, or other module at the N- and/or C-terminus [3]. Despite high structural conservation of the catalytically active core domain and catalytic machinery, α/β hydrolases exhibit a high sequence diversity and a broad variety of catalytic activities [4,5]. With sequence and structural diversity, these extra modules extending from the catalytically active core domain are responsible for determining and regulating catalytic activity, substrate specificity, and the stability of the α/β hydrolases [6–8]. The extra domain has been the hotspot for enzyme engineering of enzymatic properties such as catalytic activity and thermostability [9–11].

As the typical α/β hydrolase, the esterases and lipases have been widely investigated to explore the sequence-structure-function relationships of the α/β hydrolase fold superfamily [8,11–14]. Lid swapping for the lipase B from *Candida antarctica* elucidated the plasticity of the α/β hydrolase fold [11]. The α-helical cap domain of the esterase AsFAE from *Alistipes shahii* and the loop containing the catalytic triad Asp of the feruloyl esterase from *Lactiplantibacillus plantarum* shaped the substrate-binding pocket and unraveled the molecular mechanism of the substrate specificity [8,12]. The dimerization of the Pf2001 esterase revealed a temperature-dependent activation mechanism and was necessary for the substrate channel formation in the active site cleft [13]. The acidic surface of the esterase EstN7 from *Bacillus cohnii* N1 played a role in the cold-adaption [14]. Furthermore, the

esterases and lipases have exhibited considerable potential for a broad range of applications because of the regio- and stereoselectivity, the stability in nonpolar media, and the ability to catalysis of alcoholysis, esterification, and transesterification [15–18]. Bacterial esterases and lipases from the hormone-sensitive lipase (HSL) family corresponding to the bacterial family IV [19] typically possessed an extra cap domain extending from the catalytically active core domain and covering the active site [20,21]. It had been suggested that the extensional N-terminal module of the cap domain with various length participated in substrate binding and was important for several enzyme functions [22]. The N-terminal cap (36 residues) of the thermophilic esterase EST2 from *Alicyclobacillus acidocaldarius* played a key role in catalytic activity, substrate specificity, regioselectivity, and conformational stability [22,23]. The N-terminal domain (97 residues) of the lipase *Psy*HSL from *Psychrobacter* sp. TA144 was involved in enzyme catalysis [24].

In our previous study, the arylesterase LggEst from the probiotics *L. rhamnosus* GG (LGG) had been biochemically characterized in detail [25]. The crystal structures of both the esterase B (PDB id 4PO3 and 4OUK) from *L. rhamnosus* HN001 and the esterase B (PDB id 4N5I and 4N5H) from *L. rhamnosus* Lc705 sharing identical sequence with LggEst had been determined and deposited into the Protein Data Bank [26]. These structures exhibited that the arylesterase LggEst possessed the catalytically active core domain with a canonical α/β hydrolase fold and an extra module at the N-terminus consisting of only an extensional long α-helix (28 residues, Ala2-Glu29) and extending from the catalytically active core domain. In this study, we focused on the role of the N-terminal extensional long α-helix (NEL-helix) in the arylesterase LggEst on catalysis and stability.

2. Results and Discussion

2.1. Location of N-Teminal Extensional Long α-Helix (NEL-Helix)

A structural analysis for ten bacterial esterases [21,26–34] from the GDSAG motif subfamily [35] of the HSL family exhibited that this group of esterases were comprised of the catalytic active core domain with the canonical α/β hydrolase fold and an extra domain (Figure 1), similar to other members of the α/β hydrolase fold superfamily. Especially, the extra cap domain of these esterases was composed of one α-helix or two short α-helices (α1-2) locating at the N-terminus and two short α-helices (α6-7) positioning between the strands β6 and β7 (Figure 1), and covered the active site consisting of the catalytic triad Ser-Asp-His with the conserved serine motif of GDSAG and the GGGX-type oxyanion hole (Figure 1A). The functional role of N-terminal module with two short α-helices (Figure 1B) in the thermophilic esterase EST2 from *A. acidocaldarius* had been reported [22,23].

The complex structure of the esterase B from *L. rhamnosus* HN001 sharing identical sequence with the arylesterase LggEst showed that the catalytically active core domain possessed a canonical α/β hydrolase fold consisting of a mostly parallel, eight-stranded β-sheet surrounded by α-helices on both sides (Figure 2A). Unlike the other bacterial esterases from the GDSAG motif subfamily containing one α-helix or two short α-helices at the N-terminus, only a long α-helix (28 residues, Ala2-Glu29) at the N-terminus in the arylesterase LggEst acted as the extra module extending from the catalytically active core domain to its top (Figure 2A). Furthermore, the NEL-helix of LggEst participated in the formation of the shallow substrate binding pocket (Figure 2B), such as the residues Ser14, Trp15, Thr18, and Arg21 (Figure 2C). Structural analysis for the α/β-hydrolases displayed that most cap domains formed the top part of the substrate binding site [3].

To probe into the role of the NEL-helix in the arylesterase LggEst on catalysis and stability in the HSL family, the deleted mutant ΔNEL-helix was constructed. To prevent the influence of the N-terminal $(His)_6$-tag on the role of this N-terminal α-helix, the arylesterase LggEst wild type and the deleted mutant had been successfully cloned into the vector pET-28a with the C-terminal $(His)_6$-tag (Figure S1 in Supplementary Materials), and purified to homogeneity with Ni-NTA affinity chromatography by the analysis of SDS-PAGE (Figure S2 in Supplementary Materials). Although enzymatic properties of the arylesterase LggEst with the N-terminal $(His)_6$-tag had been reported previously [25], the arylesterase LggEst

wild type with the C-terminal $(His)_6$-tag would still be characterized as the comparison with the deleted mutant in this study.

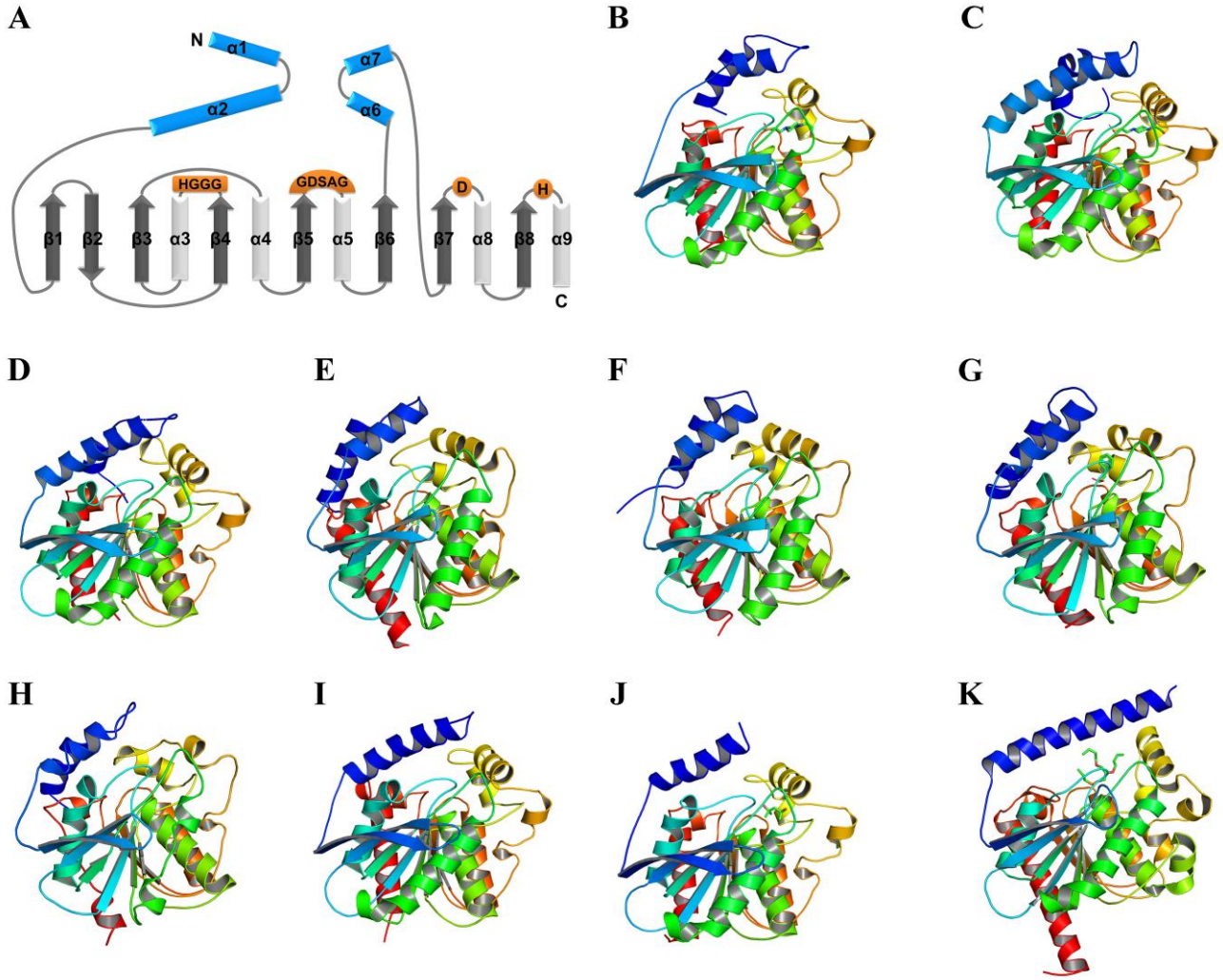

Figure 1. The overall structures of bacterial esterases belonging to the HSL family. (**A**) Secondary structures topology diagram of the HSL family. The α-helices and β-sheets are represented by cylinders and arrows, respectively. The catalytically core domain is shown in gray and white, and the additional modules are shown in blue. The locations of the conserved residues of the catalytic machinery are shown in orange. (**B**) The 3D structure of arylesterase EST2 (1EVQ) from *A. acidocaldarius* [27]. (**C**) The 3D structure of arylesterase AFEST (1JJI) from *Archaeoglobus fulgidus* [28]. (**D**) The 3D structure of the esterase PestE (2YH2) from *Pyrobaculum calidifontis* VA1 [29]. (**E**) The 3D structure of the esterase EstE7 (3DNM) from a metagenomic library [30]. (**F**) The 3D structure of the esterase E40 (4XVC) from a marine sedimental metagenomic library [31]. (**G**) The 3D structure of the esterase EstE5 (3FAK) from a soil metagenomic library [32]. (**H**) The 3D structure of the esterase EstD11 (7AT0) from a hot spring metagenomic library [21]. (**I**) The 3D structure of the esterase EstE1 (2C7B) from metagenomic library [33]. (**J**) The 3D structure of the esterase Sto-Est (3AIK) from *Sulfolobus tokodaii* 7 [34]. (**K**) The 3D structure of the esterase B (4PO3) from *L. rhamnosus* HN001 [26]. These structural images are generated using the software PyMOL [36].

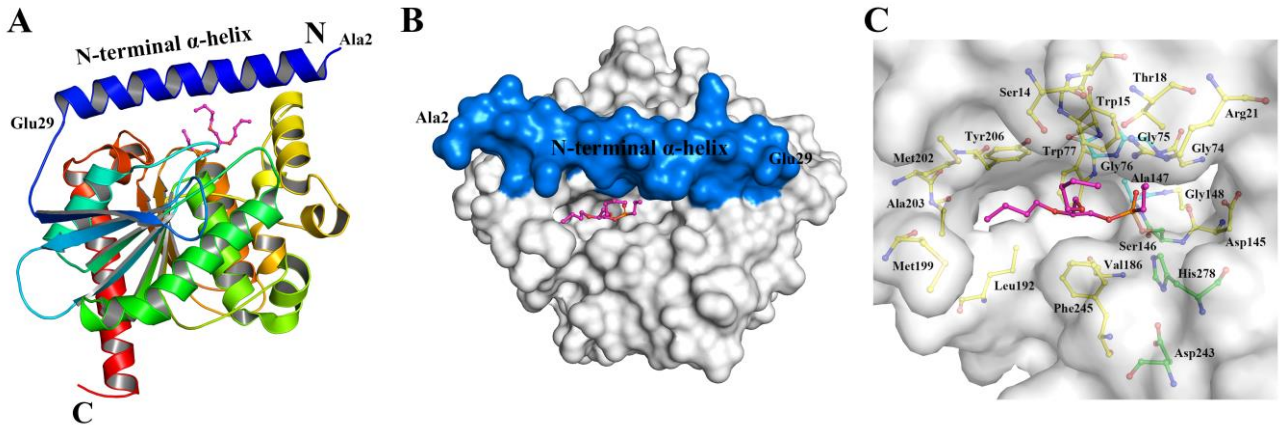

Figure 2. Location of N-terminal extensional long α-helix of arylesterase LggEst shown in cartoon (**A**) and surface (**B**), and the substrate binding cleft of LggEst (**C**). N-terminal extensional α-helix (Ala2-Glu29) is shown in blue. The ligand (2*R*)-2,3-dibutoxypropyl hydrogen (*S*)-propylphosphonate (HY4) is shown in pink ball and sticks. The catalytic triad are shown in green ball and sticks. The residues serving as the oxyanion hole are shown in cyan ball and sticks. These structural images of LggEst are generated using the software PyMOL based on 3D structure (PDB id: 4PO3) of the homologue esterase B from *L. rhamnosus* HN001.

2.2. Role of the NEL-Helix on Overall Structure

The secondary structures of the arylesterase LggEst wild type and the deleted mutant ΔNEL-helix had been investigated by CD. The far-UV CD spectra had a maximal peak at 195 nm and a minimal peak at 210–220 nm (Figure 3). It had been indicated that LggEst wild type and the deleted mutant maintained the α/β hydrolase fold and the deletion of the NEL-helix did not change the overall structure of this enzyme. The decrease in the peak of the deleted mutant at 195 nm showed that the deletion of the NEL-helix reduced the α-helical content of this arylesterase (Figure 3).

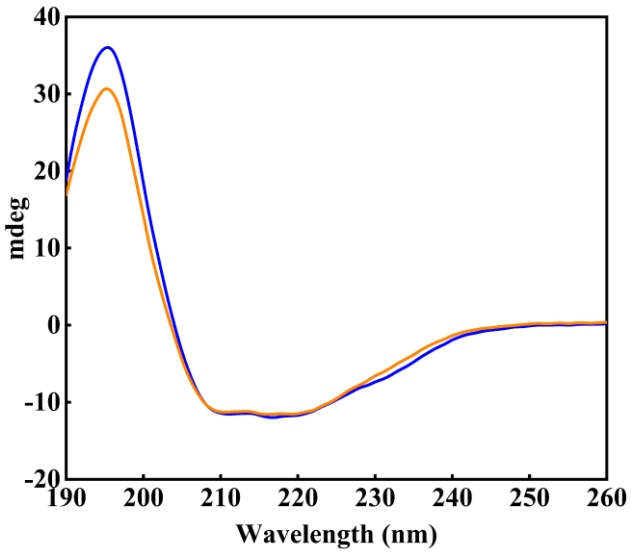

Figure 3. Far−UV CD spectra of arylesterase LggEst wild type and the deleted mutant. CD spectra were recorded from 190 to 260 nm. The spectra of wild type and the deleted mutant are shown in blue and orange, respectively. Protein concentration of 0.1 mg mL^{-1} was used for the analysis.

2.3. Role of the NEL-Helix on Optimum pH and Temperature

Arylesterase LggEst wild type and the deleted mutant possessed an optimum pH in 6.5 and 5.5, respectively (Figure 4A). Wild type showed higher activity in neutral and basic pH compared with the deleted mutant, and maintained the activity of 54–98% in

pH 7–9. However, the deleted mutant displayed high activity (>79%) in acidic pH 4.5–6.5, and retained the activity of 63% even in pH 4.0. The deletion of the NEL-helix improved catalytic ability of this enzyme LggEst in acidic pH 4–6.

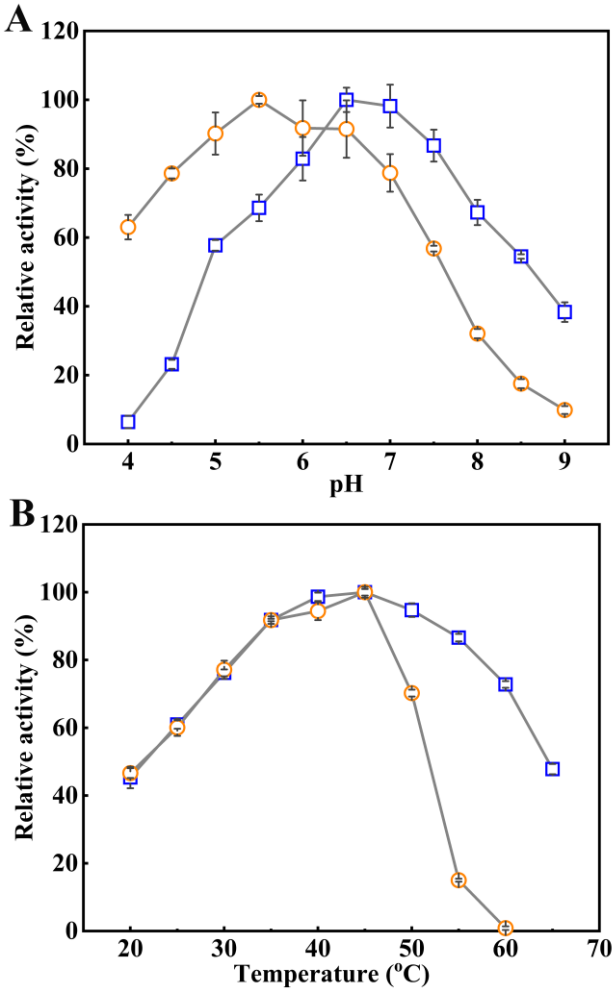

Figure 4. Effects of pH and temperature on enzymatic activities of arylesterase LggEst wild type and the deleted mutant. (**A**). Effects of pH on enzymatic activities of LggEst wild type and the deleted mutant at 45 °C under pH 4–9. Enzymatic activities of wild type and the deleted mutant are normalized as percentages of maximum activity in pH 6.5 and pH 5.5, respectively. (**B**) Effects of temperature on enzymatic activities of LggEst wild type and the deleted mutant in 50 mM NaH_2PO_4-Na_2HPO_4 buffer (pH 7.5) at 20–65 °C. Enzymatic activities are normalized as percentages of maximum activity at 45 °C. The data for wild type and the deleted mutant are shown in blue square and orange circle, respectively. All reactions were performed in triplicate, and error bars represent the standard deviations of mean.

Arylesterase LggEst wild type and the deleted mutant presented the highest activities at 45 °C (Figure 4B). Wild type and the deleted mutant displayed similar activities at the temperatures ranging from 20 to 45 °C. Wild type maintained considerable activity (73%) at 60 °C and the activity of 48% even at 65 °C (Figure 4B). However, enzymatic activity of the deleted mutant was reduced dramatically at high temperatures (55 and 60 °C) and the deleted mutant was almost inactive at 60 °C. It had been suggested the deletion of the NEL-helix resulted in a marked decrease in catalytic activity of this enzyme at high temperatures. The N-terminal α-helix of acylpeptide hydrolase from *Aeropyrum pernix* K1 and N-terminal region of the esterase E34Tt from *Thermus thermophilus* HB27 had been proven to play an important role in hyperthermophilic activity [37,38].

2.4. Role of the NEL-Helix on Catalysis and Selectivity of Acyl Chain Length

The role of the NEL-helix on catalysis and substrate selectivity of the arylesterase LggEst had been explored. Enzyme kinetic parameters of LggEst wild type and the deleted mutant on *p*NP esters with the acyl chain of different lengths from C2 to C12 were determined at 45 °C in pH 7.5 (Table 1, Figures S3 and S4 in Supplementary Materials LggEst wild type might efficiently hydrolyze the *p*NP esters from *p*NPC2 to *p*NPC10 with the V_{max} of 28.6 to 102.8 μmol min^{-1} mg^{-1}, corresponding to the turnover numbers k_{cat} of 17.4 to 62.7 s^{-1}. The deleted mutant resulted to be active on *p*NP esters, but exhibited lower catalytic activity and the k_{cat} decreased 3.7–14.3 folds compared with wild type. It had been revealed that the NEL-helix played an important role in catalytic activity of this arylesterase. The residues Ser14, Trp15, Thr18, and Arg21 located at the NEL-helix participated in the formation of the shallow substrate binding pocket (Figure 2B,C), and deletion of the NEL-helix might change the shape and size of the substrate binding pocket. Some studies have suggested that the N-terminal extensional α-helix affected the catalytic activity of bacterial esterases and lipases from the HSL family. The deletion of N-terminal two α-helices (36 residues) in the esterase EST2 from *A. acidocaldarius* resulted in a 8.4-fold decrease in k_{cat} on the *p*NPC6 [22]. This deleted mutant with the deletion of 97 residues at the N-terminus in the HSL lipase from *Psychrobacter* sp. TA144 was inactive [24]. However, some enzymes did not agree with this conclusion. The N-terminal extension of the indole-3-glycerol phosphate synthase did not affect enzymatic activities [39], and the truncation of N-terminus of the phenylalanine hydroxylase from *Chromobacterium violaceum* improved catalytic activity [40].

Table 1. Michaelis-Menten kinetic parameters of recombinant LggEst wild type and the deleted mutant.

	LggEst Wild Type				LggEst Deleted Mutant			
Substrate	**V_{max} (μmol min^{-1} mg^{-1})**	**k_{cat} (s^{-1})**	**K_M (μM)**	**k_{cat}/K_M (M^{-1} s^{-1})**	**V_{max} (μmol min^{-1} mg^{-1})**	**k_{cat} (s^{-1})**	**K_M (μM)**	**k_{cat}/K_M (M^{-1} s^{-1})**
*p*NPC2	61.6 ± 2.3	37.6 ± 1.4	$7.8 \times 10^3 \pm 0.6 \times 10^3$	4.8×10^3	16.1 ± 0.9	9.0 ± 0.5	$11.2 \times 10^3 \pm 1.1 \times 10^3$	8.0×10^2
*p*NPC4	52.5 ± 2.6	32.0 ± 1.6	$1.2 \times 10^3 \pm 0.1 \times 10^3$	2.7×10^4	14.7 ± 0.8	8.2 ± 0.4	$1.5 \times 10^3 \pm 0.2 \times 10^3$	5.5×10^3
*p*NPC6	87.2 ± 7.5	53.2 ± 4.5	247.1 ± 32.2	2.2×10^5	25.5 ± 2.6	14.2 ± 1.5	433.4 ± 58.3	3.3×10^4
*p*NPC8	102.8 ± 5.1	62.7 ± 3.1	19.6 ± 2.6	3.2×10^6	7.8 ± 0.2	4.4 ± 0.1	12.7 ± 1.3	3.5×10^5
*p*NPC10	28.6 ± 0.8	17.4 ± 0.5	4.5 ± 0.5	3.9×10^6	2.7 ± 0.1	1.5 ± 0.1	3.9 ± 0.4	3.8×10^5
*p*NPC12	3.5 ± 0.1	2.0 ± 0.1	4.0 ± 0.2	5.0×10^5	$4.5 \times 10^{-1} \pm 0.1 \times 10^{-1}$	$2.5 \times 10^{-1} \pm 0.1 \times 10^{-1}$	3.1 ± 0.2	8.1×10^4

Deletion of the NEL-helix increased the Michaelis constants K_M of this arylesterase on the esters with short and medium acyl chains (*p*NPC2, *p*NPC4, and *p*NPC6), but slightly improved the affinities on the esters with medium and long acyl chains (*p*NPC8, *p*NPC10, and *p*NPC12) (Table 1). NEL-helix of this arylesterase regulated the substrate affinity in catalysis, which could be caused by the deletion of this long α-helix enlarged the substrate binding cleft (Figure 2B). N-terminal two α-helices of the esterase EST2 from *A. acidocaldarius* affected the affinity towards *p*NPC6 [22]. N-terminal extension of the indole-3-glycerol phosphate synthases was important for substrate affinity in catalysis [41]. Both LggEst wild type and the deleted mutant displayed the highest catalytic efficiency k_{cat}/K_M towards *p*NPC10, and thus NEL-helix did not affect the selectivity of acyl chain length, although the deletion of this long α-helix afforded a 10.3-fold decrease in catalytic efficiency towards the preferred substrate *p*NPC10 (Table 1). The deletion of N-terminal two α-helices in the esterase EST2 from *A. acidocaldarius* produced a 104-fold decrease in catalytic efficiency on *p*NPC6 [22].

2.5. Role of the NEL-Helix on Thermal and Chemical Stability

The N-terminal region was critical for the stability of thermophilic esterases [22,37,40]. Enzyme inactivation experiments had been performed in order to explore the role of NEL-

helix on the stability of this arylesterase. Thermal and GdnHCl-induced inactivation curves showed that the deletion of the NEL-helix significantly reduced thermal and chemical stability of this arylesterase (Figure 5A,C). LggEst wild type still retained the activities of 90.3% after incubation for 30 min at 45 °C, but residual activity of the deleted mutant was only 4.6% after incubation for 30 min at 45 °C (Figure 5A). As in thermal inactivation tests, LggEst wild type exhibited better chemical resistance than the deleted mutant. After the treatment with 0.6 M of GdnHCl for 2 h, LggEst wild type and the deleted mutant retained 61.4% and 1.8% of original activity, respectively (Figure 5C). The C_{50} value of the deleted mutant decreased by 0.52 M compared with wild type (Table 2). The NEL-helix was crucial for stabilizing this enzyme in proper conformation for optimal catalytic activity, as the highly conserved N-terminal region of the firefly *Photinus pyralis* luciferase [42].

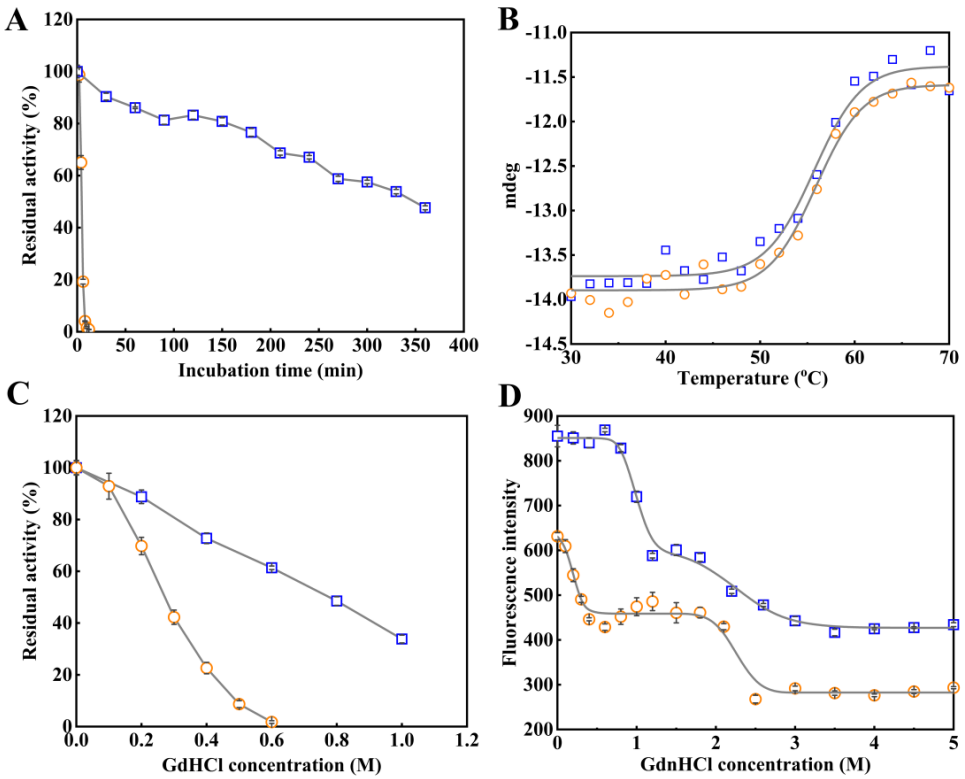

Figure 5. Thermal and chemical stabilities of arylesterase LggEst wild type and the deleted mutant. (**A**) Thermal inactivation profiles of LggEst wild type and the deleted mutant. After incubating the enzymes (1.0 mg mL^{-1}) for specified time intervals at 45 °C, the residual activities were measured in 50 mM phosphate buffer (pH 7.5) at 45 °C using *p*NPC8 as the substrate. Enzymatic activity of LggEst without incubation is taken as the 100%. All reactions were performed in triplicate, and error bars represent the standard deviations of mean. (**B**) Thermal unfolding of LggEst wild type and the deleted mutant monitored by CD scanning. Protein concentration of 1.0 mg mL^{-1} was used for the analysis. Denaturizing curves were recorded from 30 °C to 70 °C with a rate of 1 °C min^{-1}. The fitted curves for protein unfolding were shown in gray solid lines. (**C**). GdnHCl−induced inactivation of LggEst wild type and the deleted mutant. After 2 h of incubation with varied concentrations of GdnHCl at room temperature, the residual activities were measured in 50 mM phosphate buffer (pH 7.5) at 45 °C using *p*NPC8 as the substrate. All reactions were performed in triplicate, and error bars represent the standard deviations of mean. (**D**) GdnHCl−induced unfolding of LggEst wild type and the deleted mutant monitored by fluorescence spectrophotometry. The fluorescence spectra were recorded at the wavelengths between 300 and 400 nm with an excitation wavelength at 290 nm under a scanning speed of 1200 nm min^{-1}. The fitted curves for protein unfolding were shown in gray solid lines. The measured data for LggEst wild type and the deleted mutant are shown in blue square and orange circle, respectively.

Table 2. Thermodynamic parameters for enzyme inactivation and protein unfolding of LggEst wild type and the deleted mutant.

Enzymes	C_{50} (M)	T_m (°C)	C_{m1} (M)	C_{m2} (M)
LggEst wild type	0.76	55.7	1.2	2.3
LggEst deleted mutant	0.24	55.9	0.2	1.9

Furthermore, in order to clarify the role of this long α-helix on conformational stability, thermal and chemical unfolding of LggEst wild type and the deleted mutant were investigated by CD and fluorescence spectrometry. Thermal unfolding curves (Figure 5B) showed that the melting temperature T_m of the deleted mutant was similar to that of wild type (Table 2). This was consistent with the results from GdnHCl-induced unfolding using fluorescence spectrometry by monitoring the microenvironment of the tryptophan (Figure 5D). The deleted mutant presented slightly lower C_{m2} value than wild type, although the C_{m1} value of the deleted mutant was considerably lower than that of wild type. It had been revealed that the deletion of NEL-helix did not change the overall rigidity of enzyme structure. Together with the decreased thermostability and chemical resistance, these results suggested that the destabilizing effect of the deletion of the NEL-helix might come from the decreased local rigidity of the active site. The α-helix was rigid, thus the deletion of this long α-helix could decrease local rigidity of the active site. The introduction of an extra α-helix at the C-terminus was a strategy for the xylanase to improve the thermostability [43].

2.6. Role of the NEL-Helix on Organic Solvents and DOC Tolerance

The effects of various organic solvents on catalytic activity of LggEst wild type and the deleted mutant have been investigated. LggEst wild type exhibited the remarkable tolerance on eight organic solvents at the concentration of 5% and kept 48–108% of activity (Figure 6). However, catalytic activity of the deleted mutant was markedly inhibited by most organic solvents except for ethylene glycol (Figure 6). Therefore, NEL-helix was essential for this arylesterase to maintain the resistance on organic solvents.

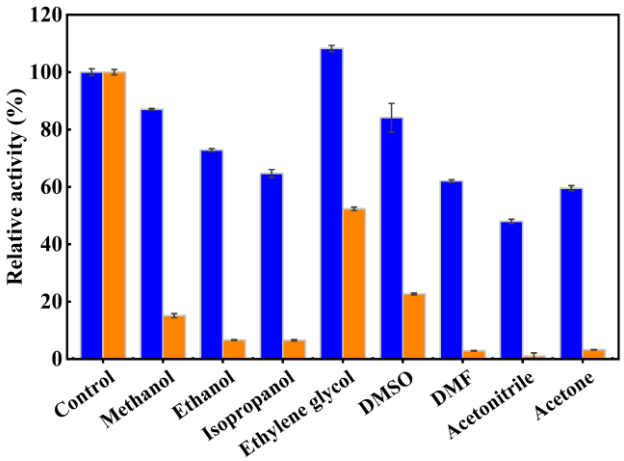

Figure 6. Effects of organic solvent on enzymatic activities of arylesterase LggEst wild type and the deleted mutant. Enzymatic activity by adding the corresponding volume of water is taken as the control. All reactions were performed in triplicate, and error bars represent the standard deviations of mean. The enzymatic activities for LggEst wild type and the deleted mutant are shown in blue and orange, respectively.

It was previously reported that enzymatic activity of this arylesterase LggEst with an N-terminal $(His)_6$-tag was improved by ionic detergent DOC at the temperatures ranging from 30 to 65 °C [25]. An amount of 0.1% (*w*/*v*) DOC enhanced the activity of LggEst wild type with a C-terminal $(His)_6$-tag at higher temperatures (45–65 °C) (Figure 7A), and 0.1%

(*w*/*v*) DOC produced a remarkable increase in catalytic activity of the deleted mutant at a wider temperature range (20–60 °C) (Figure 7B). The presence of 0.1% (*w*/*v*) DOC partially replenished the loss of catalytic activity of this arylesterase caused by the deletion of the NEL-helix.

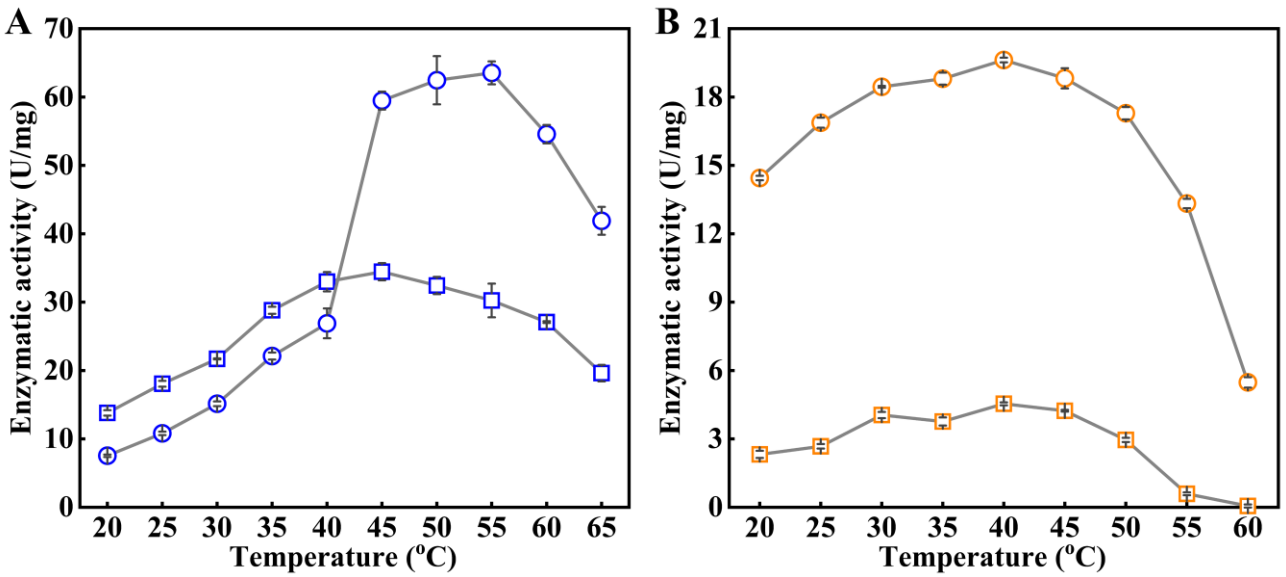

Figure 7. Effects of 0.1% (*w*/*v*) DOC on enzyme activity of arylesterase LggEst wild type and the deleted mutant at different temperatures. (**A**) Effects of 0.1% (*w*/*v*) DOC on enzyme activity of LggEst wild type at 20–65 °C. The enzymatic activities without and with 0.1% (*w*/*v*) DOC are shown in blue square and circle, respectively. (**B**) Effects of 0.1% (*w*/*v*) DOC on enzyme activity of arylesterase LggEst deleted mutant at 20–60 °C. The enzymatic activities without and with 0.1% (*w*/*v*) DOC are shown in orange square and circle, respectively. Enzymatic activity by adding the corresponding volume of 50 mM NaH_2PO_4-Na_2HPO_4 buffer (pH 7.5) was taken as the control. All reactions were performed in triplicate, and error bars represent the standard deviations of mean.

3. Materials and Methods

3.1. Bacterial Strains, Enzymes and Reagents

Oligonucleotide primers were synthesized by Sangon Biotech (Shanghai, China). *TransStart*® *FastPfu* Fly DNA polymerase and PCR related reagents were purchased from TransGen Biotech (Beijing, China). *Escherichia coli* DH5α was used as the host for gene cloning, and *E. coli* BL21(DE3) was used for protein over-expression. The substrates *p*-nitrophenyl acetate (*p*NPC2), *p*-nitrophenyl butyrate (*p*NPC4), *p*-nitrophenyl caprylate (*p*NPC8), *p*-nitrophenyl caprate (*p*NPC10), and *p*-nitrophenyl laurate (*p*NPC12) used for enzyme activity assay and kinetics were purchased from Sigma-Aldrich (St. Louis, MO, USA) except that *p*-nitrophenyl hexanoate (*p*NPC6) was provided by Tokyo Chemical Industry (Shanghai, China). Isopropyl-β-D-thiogalactoside (IPTG), kanamycin, imidazole, and guanidine hydrochloride (GdnHCl) were purchased from Sangon Biotech (Shanghai, China). Other chemicals for buffer and medium preparation were of analytical grade or higher.

3.2. Gene Cloning, Over-Expression and Purification

The arylesterase LggEst wild type and the deleted mutant genes were cloned into the vector pET-28a by the method prolonged overlap extension polymerase chain reaction (POE-PCR) [44], as previously described [45], by using the primers as listed in Table S1 in Supplementary Materials. The POE-PCR products were directly transformed into *E. coli* DH5α. The sequence of LggEst wild type and the deleted mutant genes were confirmed by DNA sequencing (Sangon Biotech, Shanghai, China). The over-expression of LggEst wild type and the deleted mutant in *E. coli* BL21(DE3) were induced for overnight at 16 °C by

addition of 0.5 mM IPTG until OD600 reached 2.0. Then, the BL21(DE3) cells were harvested and resuspended in 50 mM phosphate buffer (pH 8.0) containing 12 mM imidazole, and then disrupted by sonication for 60 min by working for 2 s with an interval of 3 s. After sonication, the cell lysate was cleared by centrifugation at 9000× *g* for 30 min at 4 °C. The recombinant LggEst wild type and the deleted mutant was purified by Ni-NTA affinity chromatography (Qiagen, Hilden, Germany). The purified LggEst was further dialyzed twice in 50 mM phosphate buffer (pH 8.0). Protein concentrations were measured at 280 nm by NanoDrop 2000 UV-vis spectrophotometer (Thermo Fisher Scientific, Waltham, MA, USA).

3.3. Circular Dichroism (CD) Spectroscopy

Far-UV CD spectra of LggEst wild type and the deleted mutant were monitored by Chirascan qCD spectropolarimeter (Applied Photophysics, Leatherhead, UK) from 190 to 260 nm at room temperature with the following parameters: protein concentration 6.0 μM, bandwidth 1.0 nm, data interval 1.0 nm, pathlength 1.0 cm, and scanning speed 30 nm min^{-1}. Each scan was repeated three times and the average value was used for analysis. The baseline was measured by using 50 mM phosphate buffer (pH 8.0).

3.4. Enzyme Activity Assay

The enzyme activity assays had previously been described [25]. Enzymatic activities were measured by instantaneously monitoring the release of *p*-nitrophenol from the substrate *p*NPC8 at 405 nm in 50 mM phosphate buffer (pH 7.5) using an UV-5800PC spectrophotometer (METASH, Shanghai, China) equipped with a thermal controller, except that the effect of pH on enzymatic activity was determined by termination method. One unit of enzyme activity (U) was defined as the amount of enzyme releasing 1 μmol *p*-nitrophenol from the substrate per min at 45 °C in pH 7.5. All assays were performed in triplicate.

3.5. Effects of pH and Temperature on Activity

The effects of pH on enzymatic activities of LggEst wild type and the deleted mutant were determined at 45 °C in 30 mM wide range buffer ranging from pH 4.0 to pH 11.0 as previously described [25]. The wide range buffer contained 30 mM each of 4-(2-hydroxyethyl)-1-piperazineethanesulfonic acid (HEPES), 3-[[1,3-dihydroxy-2-(hydroxymethyl)propan-2-yl]amino]propa-ne-1-sulfonic acid (TAPS), 3-(cyclohexylamino)-1-propanesulfonicacid (CAPS), 2-(N-morpholino)ethanesulfonic acid (MES), and acetic acid, and was adjusted to the appropriate pH with 1 M NaOH at 45 °C. The effects of temperatures on the enzymatic activity of LggEst wild type and the deleted mutant were determined at the temperature ranges from 20 to 65 °C and from 20 to 60 °C, respectively.

3.6. Enzyme Steady-State Kinetics

Enzyme kinetics of LggEst wild type and the deleted mutant for the substrates *p*NPC2, *p*NPC4, *p*NPC6, *p*NPC8, *p*NPC10, and *p*NPC12 were determined. For the *p*-nitrophenyl esters with different acyl chain lengths, appropriate substrates concentrations ranges and appropriate enzyme concentrations were used for measuring the initial rate of hydrolysis reaction. Kinetic parameters V_{max} and K_M were acquired by fitting catalytic activities as a function of substrate concentrations to the Michaelis-Menten equation using non-linear regression of the software GraphPad Prism 6. The parameter k_{cat} was obtained by using the equation $k_{cat} = V_{max}/[E]$, where [E] was the molar concentration of the enzyme.

3.7. Thermal Inactivation and Thermal Unfolding for Arylesterase

Thermal inactivation experiments of LggEst wild type and the deleted mutant were performed by pre-incubating the enzymes (1.0 mg mL^{-1}) for specified time intervals at 45 °C. The enzyme samples were then cooled on ice and residual activities were measured.

Thermal unfolding measurements of LggEst wild type and the deleted mutant were carried out by detecting the change of mdeg value at 222 nm using Chirascan qCD

spectropolarimeter (Applied Photophysics, London, UK). A protein concentration of 0.2 mg mL^{-1} was used. Denaturizing curves were recorded from 30 to 70 °C at a rate of 2 °C min^{-1}. The baseline scan was measured using 50 mM phosphate buffer (pH 8.0). The thermograms (mdeg versus temperature) were analyzed using a two-state model in which the melting temperature (T_m) was fitted using the software 1stopt.

3.8. Chemical Inactivation and Chemical Unfolding Induced by GdnHCl

The inactivation of LggEst wild type and the deleted mutant induced by guanidine hydrochloride (GdnHCl) was performed by incubating the proteins (final concentration of 0.1 and 0.8 mg mL^{-1} for wild type and the deleted mutant, respectively) with a set of concentrations of GdnHCl for 2 h at room temperature. The residual activities were measured in 50 mM phosphate buffer (pH 7.5) containing the corresponding concentration of GdnHCl. The C_{50}, which indicates the concentration of GdnHCl capable of inhibiting 50% of the catalytic activity, was estimated as previously described [46].

Chemical unfolding induced by GdnHCl was performed by incubating 0.1 mg mL^{-1} of proteins with a list of concentrations (0.0–5.0 M) of GdnHCl for 12 h at room temperature. The GdnHCl-induced unfolding for LggEst wild type and the deleted mutant were monitored using a fluorescence spectrophotometer LS55 (PerkinElmer, Waltham, MA, USA) with an excitation wavelength of 290 nm at 25 °C. The fluorescence spectra were recorded at the wavelengths between 300 and 400 nm at a scanning speed of 300 nm min^{-1}. The unfolding experiments were performed twice and the processed data were given as the means of two measurements. The data for wild type and the deleted mutant were analyzed by a three-state model using the software 1stopt 3.0. The C_m, the GdnHCl concentration at the midpoint of the GdnHCl-induced unfolding curve, were obtained as previously described [46].

3.9. Effects of Organic Solvents and Sodium Deoxycholate (DOC) on Activity

The effects of organic solvents on enzymatic activity of arylesterase LggEst wild type and the deleted mutant were determined by measuring catalytic activities in the standard assay described above using *p*NPC8 as the substrate with 10% and 20% (*v*/*v*) of various organic solvents.

The effects of DOC on enzymatic activity of arylesterase LggEst wild type and the deleted mutant at different temperatures were determined by measuring catalytic activities in the standard assay described above using *p*NPC8 as the substrate with 0.1% (*w*/*v*) DOC at different temperatures.

4. Conclusions

Unlike the other bacterial esterases from the GDSAG motif subfamily of the HSL family using one or two short α-helices as a part of the cap domain at the N-terminus, only a long α-helix (Ala2-Glu29, NEL-helix) in the arylesterase LggEst acted as the N-terminal module of the cap domain extending from the catalytically active core domain to its top and participated in the formation of the shallow substrate binding cleft. The deletion of the NEL-helix did not change the overall structure of this arylesterase. The deletion of the NEL-helix led to the shifting of optimal pH into the acidity and the loss of thermophilic activity. The NEL-helix played an important role in catalytic activity and did not affect the selectivity of the acyl chain length. The NEL-helix was crucial for thermostability, chemical resistance, and the tolerance towards organic solvents. However, the deletion of NEL-helix did not change the rigidity of the overall structure and only reduced the local rigidity of the active site. The present work elucidated the role of the NEL-helix on catalysis and stability in the HSL family.

Supplementary Materials: The following supporting information can be downloaded at: https://www.mdpi.com/article/10.3390/catal13020441/s1, Table S1: PCR primers used for cloning of the arylesterase LggEst wild type and deleted mutant into the plasmid pET-28a; Figure S1: Gene cloning

of the arylesterase LggEst wild type and deleted mutant; Figure S2: SDS-PAGE (15%) for purification of recombinant LggEst wild type and the deleted mutant in *E. coli* BL21(DE3); Figure S3. Michaelis-Menten kinetic plots for arylesterase LggEst wild type on the hydrolysis of the *p*-nitrophenyl esters; Figure S4. Michaelis-Menten kinetic plots for arylesterase LggEst deleted mutant on the hydrolysis of the *p*-nitrophenyl esters.

Author Contributions: Conceptualization, B.-C.L.; funding acquisition, B.-C.L.; methodology, B.-C.L., T.G., X.L. and X.H.; formal analysis, T.G., X.L. and X.H.; investigation, T.G.; data curation, T.G.; visualization, B.-C.L. and T.G.; writing—original draft, B.-C.L. and G.-B.D.; writing—review and editing, B.-C.L. and G.-B.D.; supervision, B.-C.L. All authors have read and agreed to the published version of the manuscript.

Funding: This work was supported by the Natural Science Foundation of Shanxi for Applied and Basic Research Program (No. 201901D111013).

Data Availability Statement: Not applicable.

Conflicts of Interest: The authors declare no conflict of interest.

References

1. Nardini, M.; Dijkstra, B.W. α/β Hydrolase fold enzymes: The family keeps growing. *Curr. Opin. Struct. Biol.* **1999**, *9*, 732–737. [CrossRef]
2. Heikinheimo, P.; Goldman, A.; Jeffries, C.; Ollis, D.L. Of barn owls and bankers: A lush variety of α/β hydrolases. *Structure* **1999**, *7*, R141–R146. [CrossRef]
3. Bauer, T.L.; Buchholz, P.C.F.; Pleiss, J. The modular structure of α/β-hydrolases. *FEBS J.* **2020**, *287*, 1035–1053. [CrossRef] [PubMed]
4. Rauwerdink, A.; Kazlauskas, R.J. How the same core catalytic machinery catalyzes 17 different reactions: The serine-histidine-aspartate catalytic triad of α/β-hydrolase fold enzymes. *ACS Catal.* **2015**, *5*, 6153–6176. [CrossRef] [PubMed]
5. Holmquist, M. Alpha/beta-hydrolase fold enzymes: Structures, functions and mechanisms. *Curr. Protein. Pept. Sci.* **2000**, *1*, 209–235. [CrossRef] [PubMed]
6. Khan, F.I.; Lan, D.; Durrani, R.; Huan, W.; Zhao, Z.; Wang, Y. The lid domain in lipases: Structural and functional determinant of enzymatic properties. *Front. Bioeng. Biotechnol.* **2017**, *5*, 16. [CrossRef]
7. Miled, N.; Bussetta, C.; De caro, A.; Rivière, M.; Berti, L.; Canaan, S. Importance of the lid and cap domains for the catalytic activity of gastric lipases. *Comp. Biochem. Physiol. B Biochem. Mol. Biol.* **2003**, *136*, 131–138. [CrossRef]
8. Wei, X.; Wang, Y.L.; Wen, B.T.; Liu, S.J.; Wang, L.; Sun, L.; Gu, T.Y.; Li, Z.; Bao, Y.; Fan, S.L.; et al. The α-helical cap domain of a novel esterase from gut *Alistipes shahii* shaping the substrate-binding pocket. *J. Agric. Food Chem.* **2021**, *69*, 6064–6072. [CrossRef]
9. Gall, M.G.; Nobili, A.; Pavlidis, I.V.; Bornscheuer, U.T. Improved thermostability of a *Bacillus subtilis* esterase by domain exchange. *Appl. Microbiol. Biotechnol.* **2014**, *98*, 1719–1726. [CrossRef]
10. Luan, Z.J.; Yu, H.L.; Ma, B.D.; Qi, Y.K.; Chen, Q.; Xu, J.H. Dramatically improved performance of an esterase for cilastatin synthesis by cap domain engineering. *Ind. Eng. Chem. Res.* **2016**, *55*, 12167–12172. [CrossRef]
11. Skjøt, M.; De Maria, L.; Chatterjee, R.; Svendsen, A.; Patkar, S.A.; Ostergaard, P.R.; Brask, J. Understanding the plasticity of the α/β hydrolase fold: Lid swapping on the *Candida antarctica* lipase B results in chimeras with interesting biocatalytic properties. *Chembiochem* **2009**, *10*, 520–527. [CrossRef] [PubMed]
12. Zhang, H.; Wen, B.; Liu, Y.; Du, G.; Wei, X.; Imam, K.M.S.U.; Zhou, H.; Fan, S.; Wang, F.; Wang, Y.; et al. A reverse catalytic triad Asp containing loop shaping a wide substrate binding pocket of a feruloyl esterase from *Lactobacillus plantarum*. *Int. J. Biol. Macromol.* **2021**, *184*, 92–100. [CrossRef] [PubMed]
13. Varejão, N.; De-Andrade, R.A.; Almeida, R.V.; Anobom, C.D.; Foguel, D.; Reverter, D. Structural mechanism for the temperature-dependent activation of the hyperthermophilic Pf2001 esterase. *Structure* **2018**, *26*, 199–208. [CrossRef]
14. Noby, N.; Auhim, H.S.; Winter, S.; Worthy, H.L.; Embaby, A.M.; Saeed, H.; Hussein, A.; Pudney, C.R.; Rizkallah, P.J.; Wells, S.A.; et al. Structure and in silico simulations of a cold-active esterase reveals its prime cold-adaptation mechanism. *Open Biol.* **2021**, *11*, 210182. [CrossRef] [PubMed]
15. Romano, D.; Bonomi, F.; de Mattos, M.C.; de Sousa Fonseca, T.; de Oliveira Mda, C.; Molinari, F. Esterases as stereoselective biocatalysts. *Biotechnol. Adv.* **2015**, *33*, 547–565. [CrossRef]
16. Bornscheuer, U.T. Microbial carboxyl esterases: Classification, properties and application in biocatalysis. *FEMS Microbiol. Rev.* **2002**, *26*, 73–81. [CrossRef]
17. Panda, T.; Gowrishankar, B.S. Production and applications of esterases. *Appl. Microbiol. Biotechnol.* **2005**, *67*, 160–169. [CrossRef]
18. Jaeger, K.E.; Eggert, T. Lipases for biotechnology. *Curr. Opin. Biotechnol.* **2002**, *13*, 390–397. [CrossRef]
19. Arpigny, J.L.; Jaeger, K.E. Bacterial lipolytic enzymes: Classification and properties. *Biochem. J.* **1999**, *343*, 177–183. [CrossRef]

20. Wei, Y.; Contreras, J.A.; Sheffield, P.; Osterlund, T.; Derewenda, U.; Kneusel, R.E.; Matern, U.; Holm, C.; Derewenda, Z.S. Crystal structure of brefeldin A esterase, a bacterial homolog of the mammalian hormone-sensitive lipase. *Nat. Struct. Biol.* **1999**, *6*, 340–345.
21. Miguel-Ruano, V.; Rivera, I.; Rajkovic, J.; Knapik, K.; Torrado, A.; Otero, J.M.; Beneventi, E.; Becerra, M.; Sánchez-Costa, M.; Hidalgo, A.; et al. Biochemical and structural characterization of a novel thermophilic esterase EstD11 provide catalytic insights for the HSL family. *Comput. Struct. Biotechnol. J.* **2021**, *19*, 1214–1232. [CrossRef]
22. Mandrich, L.; Merone, L.; Pezzullo, M.; Cipolla, L.; Nicotra, F.; Rossi, M.; Manco, G. Role of the N terminus in enzyme activity, stability and specificity in thermophilic esterases belonging to the HSL family. *J. Mol. Biol.* **2005**, *345*, 501–512. [CrossRef] [PubMed]
23. Foglia, F.; Mandrich, L.; Pezzullo, M.; Graziano, G.; Barone, G.; Rossi, M.; Manco, G.; Del Vecchio, P. Role of the N-terminal region for the conformational stability of esterase 2 from *Alicyclobacillus acidocaldarius*. *Biophys. Chem.* **2007**, *127*, 113–122. [CrossRef] [PubMed]
24. De Santi, C.; Tutino, M.L.; Mandrich, L.; Giuliani, M.; Parrilli, E.; Del Vecchio, P.; de Pascale, D. The hormone-sensitive lipase from *Psychrobacter* sp. TA144: New insight in the structural/functional characterization. *Biochimie* **2010**, *92*, 949–957. [CrossRef] [PubMed]
25. Li, B.C.; Guo, T.T.; Ding, G.B. Characteration of a novel arylesterase from probiotics *Lacticaseibacillus rhamnosus* GG with the preference for medium- and long-chain *p*-nitrophenyl esters. *3 Biotech* **2021**, *11*, 496. [CrossRef] [PubMed]
26. Velankar, S.; Burley, S.K.; Kurisu, G.; Hoch, J.C.; Markley, J.L. The Protein Data Bank archive. *Methods Mol. Biol.* **2021**, *2305*, 3–21.
27. Mandrich, L.; Menchise, V.; Alterio, V.; De Simone, G.; Pedone, C.; Rossi, M.; Manco, G. Functional and structural features of the oxyanion hole in a thermophilic esterase from *Alicyclobacillus acidocaldarius*. *Proteins* **2008**, *71*, 1721–1731. [CrossRef] [PubMed]
28. De Simone, G.; Menchise, V.; Manco, G.; Mandrich, L.; Sorrentino, N.; Lang, D.; Rossi, M.; Pedone, C. The crystal structure of a hyper-thermophilic carboxylesterase from the archaeon *Archaeoglobus fulgidus*. *J. Mol. Biol.* **2001**, *314*, 507–518. [CrossRef]
29. Palm, G.J.; Fernández-Álvaro, E.; Bogdanović, X.; Bartsch, S.; Sczodrok, J.; Singh, R.K.; Böttcher, D.; Atomi, H.; Bornscheuer, U.T.; Hinrichs, W. The crystal structure of an esterase from the hyperthermophilic microorganism *Pyrobaculum calidifontis* VA1 explains its enantioselectivity. *Appl. Microbiol. Biotechnol.* **2011**, *91*, 1061–1072. [CrossRef]
30. Nam, K.H.; Kim, M.Y.; Kim, S.J.; Priyadarshi, A.; Kwon, S.T.; Koo, B.S.; Yoon, S.H.; Hwang, K.Y. Structural and functional analysis of a novel hormone-sensitive lipase from a metagenome library. *Proteins* **2009**, *74*, 1036–1040. [CrossRef] [PubMed]
31. Li, P.Y.; Chen, X.L.; Ji, P.; Li, C.Y.; Wang, P.; Zhang, Y.; Xie, B.B.; Qin, Q.L.; Su, H.N.; Zhou, B.C.; et al. Interdomain hydrophobic interactions modulate the thermostability of microbial esterases from the hormone-sensitive lipase family. *J. Biol. Chem.* **2015**, *290*, 11188–11198. [CrossRef]
32. Nam, K.H.; Kim, M.Y.; Kim, S.J.; Priyadarshi, A.; Lee, W.H.; Hwang, K.Y. Structural and functional analysis of a novel EstE5 belonging to the subfamily of hormone-sensitive lipase. *Biochem. Biophys. Res. Commun.* **2009**, *379*, 553–556. [CrossRef]
33. Byun, J.S.; Rhee, J.K.; Kim, N.D.; Yoon, J.; Kim, D.U.; Koh, E.; Oh, J.W.; Cho, H.S. Crystal structure of hyperthermophilic esterase EstE1 and the relationship between its dimerization and thermostability properties. *BMC Struct. Biol.* **2007**, *7*, 47. [CrossRef]
34. Angkawidjaja, C.; Koga, Y.; Takano, K.; Kanaya, S. Structure and stability of a thermostable carboxylesterase from the thermoacidophilic archaeon *Sulfolobus tokodaii*. *FEBS J.* **2012**, *279*, 3071–3084. [CrossRef] [PubMed]
35. Jeon, J.H.; Lee, H.S.; Kim, J.T.; Kim, S.J.; Choi, S.H.; Kang, S.G.; Lee, J.H. Identification of a new subfamily of salt-tolerant esterases from a metagenomic library of tidal flat sediment. *Appl. Microbiol. Biotechnol.* **2012**, *93*, 623–631. [CrossRef] [PubMed]
36. Delano, W.L. The PyMOL Molecular Graphics System. *DeLano Scientific* **2002**.
37. Zhang, Z.; Zheng, B.; Wang, Y.; Chen, Y.; Manco, G.; Feng, Y. The conserved N-terminal helix of acylpeptide hydrolase from archaeon *Aeropyrum pernix* K1 is important for its hyperthermophilic activity. *Biochim. Biophys. Acta.* **2008**, *1784*, 1176–1183. [CrossRef]
38. Fuciños, P.; Atanes, E.; López-López, O.; Esperanza Cerdán, M.; Isabel González-Siso, M.; Pastrana, L.; Luisa Rúa, M. Production and characterization of two N-terminal truncated esterases from *Thermus thermophilus* HB27 in a mesophilic yeast: Effect of N-terminus in thermal activity and stability. *Protein Expr. Purif.* **2011**, *78*, 120–130. [CrossRef]
39. Schneider, B.; Knöchel, T.; Darimont, B.; Hennig, M.; Dietrich, S.; Babinger, K.; Kirschner, K.; Sterner, R. Role of the N-terminal extension of the $(\beta\alpha)_8$-barrel enzyme indole-3-glycerol phosphate synthase for its fold, stability, and catalytic activity. *Biochemistry* **2005**, *44*, 16405–16412. [CrossRef]
40. Liu, Z.; Cheng, Z.; Ye, S.; Zhou, L.; Zhou, Z. Catalytic ability improvement of phenylalanine hydroxylase from *Chromobacterium violaceum* by N-terminal truncation and proline introduction. *J. Microbiol. Biotechnol.* **2019**, *29*, 1375–1382. [CrossRef] [PubMed]
41. Singh, M.K.; Shivakumaraswamy, S.; Gummadi, S.N.; Manoj, N. Role of an N-terminal extension in stability and catalytic activity of a hyperthermostable α/β hydrolase fold esterase. *Protein Eng. Des. Sel.* **2017**, *30*, 559–570. [CrossRef] [PubMed]
42. Sung, D.; Kang, H. The N-terminal amino acid sequences of the firefly luciferase are important for the stability of the enzyme. *Photochem. Photobiol.* **1998**, *68*, 749–753. [CrossRef] [PubMed]
43. Li, G.; Chen, X.; Zhou, X.; Huang, R.; Li, L.; Miao, Y.; Liu, D.; Zhang, R. Improvement of GH10 family xylanase thermostability by introducing of an extra α-helix at the C-terminal. *Biochem. Biophys. Res. Commun.* **2019**, *515*, 417–422. [CrossRef]
44. You, C.; Zhang, X.Z.; Zhang, Y.H. Simple cloning via direct transformation of PCR product DNA multimer, to *Escherichia coli* and *Bacillus subtilis*. *Appl. Environ. Microbiol.* **2012**, *78*, 1593–1595. [CrossRef]

45. Li, B.C.; Peng, B.; Zhang, T.; Li, Y.Q.; Ding, G.B. A spectrophotometric method for high-throughput screening of α-L-rhamnosidase activity on rutin coupled with a β-D-glucosidase assay. *3 Biotech* **2019**, *9*, 227. [CrossRef] [PubMed]
46. Li, B.; Yang, G.; Wu, L.; Feng, Y. Role of the NC-loop in catalytic activity and stability in lipase from *Fervidobacterium changbaicum*. *PLoS ONE* **2012**, *7*, e46881. [CrossRef]